



HAL
open science

Kinetic study and modelling of char combustion in TGA in isothermal conditions

Mathieu Morin, Sébastien Pécate, Enrica Masi, Mehrdji Hemati

► To cite this version:

Mathieu Morin, Sébastien Pécate, Enrica Masi, Mehrdji Hemati. Kinetic study and modelling of char combustion in TGA in isothermal conditions. *Fuel*, 2017, 203, pp.522-536. 10.1016/j.fuel.2017.04.134 . hal-01845490

HAL Id: hal-01845490

<https://hal.science/hal-01845490v1>

Submitted on 20 Jul 2018

HAL is a multi-disciplinary open access archive for the deposit and dissemination of scientific research documents, whether they are published or not. The documents may come from teaching and research institutions in France or abroad, or from public or private research centers.





L'archive ouverte pluridisciplinaire **HAL**, est destinée au dépôt et à la diffusion de documents scientifiques de niveau recherche, publiés ou non, émanant des établissements d'enseignement et de recherche français ou étrangers, des laboratoires publics ou privés.



OATAO is an open access repository that collects the work of Toulouse researchers and makes it freely available over the web where possible

This is an author's version published in: <http://oatao.univ-toulouse.fr/20477>

Official URL : <http://doi.org/10.1016/j.fuel.2017.04.134>

To cite this version: Morin, Mathieu  and Pecate, Sébastien 
and Masi, Enrica  and Hemati, Mehrdji  *Kinetic study and
modelling of char combustion in TGA in isothermal conditions.*
(2017) Fuel, 203. 522-536. ISSN 0016-2361

Any correspondence concerning this service should be sent
to the repository administrator: tech-oatao@listes-diff.inp-toulouse.fr

Kinetic study and modelling of char combustion in TGA in isothermal conditions

Mathieu Morin ^{a,*}, Sébastien Pécate ^a, Enrica Masi ^b, Mehrdji Hémati ^a

^aLaboratoire de Génie Chimique, Université de Toulouse, CNRS, INPT, UPS, 4 allée Emile Monso, 31432 Toulouse, France

^bUniversité de Toulouse, INPT, UPS, IMFT (Institut de Mécanique des Fluides de Toulouse), 2 allée du professeur Camille Soula, 31400 Toulouse, France

H I G H L I G H T S

- Experimental study of biomass char combustion in TGA in isothermal conditions.
- Operating conditions: $T < 400$ °C, $5065 \text{ Pa} < P_{O_2} < 21,273 \text{ Pa}$, $d_p = 25 \mu\text{m}$.
- Response of the TGA to a concentration step included in the kinetic modelling.
- The GM and the RPM are the more appropriate models to represent kinetic data.
- Activation energy of 124 kJ/mol and reaction order with respect to oxygen of 0.74.

A B S T R A C T

The purpose of this work is the kinetic study of biomass char combustion in isothermal conditions in TGA. This char was obtained from fast pyrolysis of beech bark pellet in a fluidized bed reactor at 850 °C and atmospheric pressure. Kinetic study of isothermal char combustion was performed for temperatures up to 400 °C, oxygen partial pressures ranging from 5065 to 21,273 Pa and a char particles size of 25 μm . Mass transfer effects around and within the crucible were thoroughly characterized by naphthalene vaporization. Oxygen diffusion was found to have no effect on char combustion for temperatures below 400 °C. A novel method including the transfer function of the TGA which describes the variation of oxygen partial pressure just after switching the gas from inert to reactive in the TGA was taken into consideration in the kinetic modelling. Two kinetic models (the Grain Model and the Random Pore Model) were used to determine kinetic parameters. The Grain Model was found to be in very good agreement with experimental data. Values of activation energy and reaction order with respect to oxygen are respectively equal to 124 kJ/mol and 0.74. Besides, the maximum combustion rate commonly observed in the literature during char combustion was found to be the result of the non-uniform oxygen partial pressure in the TGA at the initial stage of the char combustion.

Keywords:

Combustion
Char
Kinetic
TGA
Mass transfer

1. Introduction

With the growing environmental concern, biomass gasification is a promising alternative to fossil fuel for power generation. Recently, an increasing interest was showed for the production of methane via Methanation process and “Biomass to Fisher-Tropsch Liquids”. Biomass gasification is a thermochemical conversion occurring at high temperatures with many simultaneous reactions. It occurs in two stages: (i) a fast pyrolysis step above

350 °C in which the biomass undergoes a thermal conversion leading to the formation of volatile products either condensable (steam and tars) or non-condensable (H_2 , CO , CO_2 , CH_4 and C_2H_x) and a solid residue called char [1]; (ii) a gasification step in which the char reacts with steam and carbon dioxide at temperatures greater than 700 °C to produce syngas.

Biomass gasification is an endothermic process. To maintain a fixed temperature in the reactor, a contribution of energy is required. Two types of technology exist for biomass gasification according to the method of heat transmission [2–5]. On the one hand, the heat can be provided by “in situ” combustion. This process includes the fixed bed gasifiers (co- and counter-current) and the “bubbling fluidized bed” gasifiers. In these types of reactor, the biomass undergoes drying, pyrolysis and partial combustion of

* Corresponding author.

E-mail addresses: mathieu.morin18@gmail.com (M. Morin), sebastien.pecate@ensiacet.fr (S. Pécate), emasi@imft.fr (E. Masi), mehrdji.hemati@ensiacet.fr (M. Hémati).

The influence of oxidative temperature, oxygen partial pressure and particles size on the kinetic of biomass char combustion was widely investigated in the literature. The oxidative temperature [17,19–22] and the oxygen partial pressure [17,19,21,23–25] were found to have a strong impact on the rate of combustion which increases by raising these two parameters. Several authors [17,18,26,27] studied the influence of particles size on the char reactivity in gasification and combustion. They concluded that char particles size affects the diffusion of the gaseous reactant which may lead to a non-uniform concentration in the particle. Hence, for a fixed temperature and reactant partial pressure, the particles size influences the regime of reaction (i.e. Regime I, II). For instance, in the case of CO₂ gasification at 950 °C and a CO₂ partial pressure of 0.1 MPa, Kovacik et al. [18] reported that a particle size up to 105 μm enables to achieve a chemically controlled reaction. This is in good agreement with the works of Standish et al. [26] who concluded that the time for a complete carbon conversion with CO₂ increases with the initial particles size.

The presence of ash in the char also has an influence on its reactivity in combustion [9,17,28]. However, its effect is not well-established yet. According to Zolin et al. [28], the presence of inorganic materials in the char matrix may involve either a raise in the number of active sites in the char or a decrease in the activation energy. For example, in the case of combustion of straw and leached straw chars, they found that straw char has a significantly higher reactivity than leached straw char for temperatures up to 1000 °C. As no difference in activation energies between the two chars was observed, the authors concluded that the difference in

reactivity is due to the catalytic effect of ash which involves an increase in the number of oxidation sites. In a previous work [9], we showed that the higher amount of ash in the beech bark pellet char might explain its higher oxidative reactivity compared to beech stick char. Nevertheless, other researchers [29] mentioned that the structure of char plays a more dominant role than the catalytic effect of ash for char combustion reactivity.

The literature on the kinetic of coal char combustion is extensive and has been discussed in several reviews [7,30]. The combustion kinetic of char from pyrolysis of biomass is less studied and some works are given in Table 1 in the case of non-isothermal char combustion and in Table 2 in the case of isothermal char combustion. Tables 1 and 2 show that a wide range of biomasses (wood, straw, RDF, paper, bagasse and lignin) as well as pyrolysis conditions (temperature ranging from 500 to 1400 °C and heating rate between 3 and 18,000 °C/min) were applied to produce char. The char combustion experiments were performed mostly in TGA with heating rates between 0.5 and 20 °C/min, maximum temperatures in the range of 300–1000 °C, various oxygen partial pressures (283–21,273 Pa) and char particles size less than 500 μm.

Reactivity of char with oxygen can be described by the rate of a solid-state reaction according to the following expression [31,32]:

$$\frac{dX}{dt} = k(T_p) \cdot h(P_{O_{2,s}}) \cdot f(X) \quad (1)$$

where X , $P_{O_{2,s}}$ and T_p are respectively the conversion rate, the oxygen partial pressure at the particle surface (Pa), and the particle

Table 1
Literature review on kinetic of biomass char combustion in non-isothermal conditions.

Ref.	Pyrolysis conditions	Combustion operating conditions				Kinetic expression
		Reactor Temp. (°C)	Heating rate (°C/min)	Diam. (μm)	O ₂ (%)	
[17]	Flash carbonization reactor Corncob 1.4 MPa	TGA 300–530	5–25	5–13	20, 100	$\frac{dX}{dt} _{dev} = 7.08 \cdot 10^6 \cdot \exp\left(-\frac{111,000}{RT}\right) P_{O_2}^{0.63} (1-X)$ $\frac{dX}{dt} _{BO1} = 1.26 \cdot 10^8 \cdot \exp\left(-\frac{137,000}{RT}\right) P_{O_2}^{0.7} (1-X)^{0.41}$ $\frac{dX}{dt} _{BO2} = 1.17 \cdot 10^9 \cdot \exp\left(-\frac{151,000}{RT}\right) P_{O_2}^{0.53} (0.83+X)^{3.72} (1-X)^{0.82}$ $-\frac{dm}{dt} = 0.1 \cdot \frac{dX}{dt} _{dev} + 0.3 \cdot \frac{dX}{dt} _{BO1} + 0.47 \cdot \frac{dX}{dt} _{BO2}$
[22]	TGA, 527 °C, 5–15 °C/min Olive Husks (OH) Wheat straw (WS) Grape Residues (GR) Pine Wood (PW)	TGA 400–600	10	60–150	21	OH: $\frac{dX}{dt} = 1.22 \cdot 10^5 \cdot \exp\left(-\frac{83,500}{RT}\right) (1-X)^{1.1}$ WS: $\frac{dX}{dt} = 1.66 \cdot 10^4 \cdot \exp\left(-\frac{71,200}{RT}\right) (1-X)^{1.5}$ GR: $\frac{dX}{dt} = 6.44 \cdot 10^4 \cdot \exp\left(-\frac{78,000}{RT}\right) (1-X)^2$ PW: $\frac{dX}{dt} = 1.51 \cdot 10^6 \cdot \exp\left(-\frac{108,400}{RT}\right) (1-X)^{1.2}$
[23]	RDF, Fixed bed, 60 °C/min 500 °C 600 °C 700 °C 800 °C	TGA 600	10	–	6–21	500 °C: $\frac{dX}{dt} = 1.08 \cdot 10^{10} \cdot \exp\left(-\frac{162,000}{RT}\right) P_{O_2}^{0.64} (1-X)$ 600 °C: $\frac{dX}{dt} = 4.58 \cdot 10^9 \cdot \exp\left(-\frac{162,000}{RT}\right) P_{O_2}^{0.64} (1-X)$ 700 °C: $\frac{dX}{dt} = 2.84 \cdot 10^9 \cdot \exp\left(-\frac{162,000}{RT}\right) P_{O_2}^{0.64} (1-X)$ 800 °C: $\frac{dX}{dt} = 1.89 \cdot 10^9 \cdot \exp\left(-\frac{162,000}{RT}\right) P_{O_2}^{0.64} (1-X)$
[24]	Black paper, TGA 550 °C, 0.5–5 °C/min	TGA 550	0.5–5	–	0.28–21	$\frac{dX}{dt} = 5.67 \cdot 10^9 \cdot \exp\left(-\frac{160,000}{RT}\right) P_{O_2}^{0.78} (1-X)$
[25]	Bagasse, ASTM test	TGA 600	15	90–125	1–21	$\frac{dX}{dt} = A \cdot \exp\left(-\frac{180,000}{RT}\right) P_{O_2}^{0.65} (1-X)$
[28]	Wheat straw, TGA, 45 °C/min 700 °C 900 °C 1000 °C 1200 °C 1400 °C	TGA 1000	1–20	<150	10	700 °C: $\frac{dX}{dt} = 1.31 \cdot 10^8 \cdot \exp\left(-\frac{134,000}{RT}\right) (1-X)$ 900 °C: $\frac{dX}{dt} = 4.87 \cdot 10^5 \cdot \exp\left(-\frac{114,000}{RT}\right) (1-X)$ 1000 °C: $\frac{dX}{dt} = 6.04 \cdot 10^5 \cdot \exp\left(-\frac{106,000}{RT}\right) (1-X)$ 1200 °C: $\frac{dX}{dt} = 1.1 \cdot 10^7 \cdot \exp\left(-\frac{150,000}{RT}\right) (1-X)$ 1400 °C: $\frac{dX}{dt} = 4.54 \cdot 10^9 \cdot \exp\left(-\frac{208,000}{RT}\right) (1-X)$
[43]	Fruit Husks, vertical furnace 600 °C, 10 °C/min	TGA 900	5–20	200–500	21	$\frac{dX}{dt} = 1.485 \cdot \exp\left(-\frac{70,500}{RT}\right) (1-X)$
[44]	Beech, Furnace, 527 °C	TGA 600	5–15	<80	21	$\frac{dX}{dt} _{Devol} = 1.22 \cdot 10^7 \cdot \exp\left(-\frac{114,500}{RT}\right) (\beta - X)$ $\frac{dX}{dt} = 1.4 \cdot 10^{11} \cdot \exp\left(-\frac{182,600}{RT}\right) (1 - \beta - X)^{0.9}$

Table 2

Literature review on kinetic of biomass char combustion in isothermal conditions.

Ref.	Pyrolysis conditions	Combustion operating conditions			Kinetic expression
		Reactor Temp. (°C)	Diam (μm)	O ₂ (%)	
[19]	Prosopis Alba (PA) Prosopis caldenia (PC) Nothofagus Pumilio (NP) Lignin (L) Furnace, 610 °C, 3 °C/min	TGA 350–550	< 88	2–18	PA: $\frac{dX}{dt} = \frac{S_0}{1-p} k_0 \cdot \exp\left(-\frac{84,850}{RT}\right) P_{O_2}^{0.74} (1-X) \cdot \sqrt{1-5\ln(1-X)}$ PC: $\frac{dX}{dt} = \frac{S_0}{1-p} k_0 \cdot \exp\left(-\frac{93,200}{RT}\right) P_{O_2}^{0.8} (1-X) \cdot \sqrt{1-2.6\ln(1-X)}$ NP: $\frac{dX}{dt} = \frac{S_0}{1-p} k_0 \cdot \exp\left(-\frac{124,600}{RT}\right) P_{O_2}^{0.85} (1-X) \cdot \sqrt{1-2.6\ln(1-X)}$ L: $\frac{dX}{dt} = \frac{S_0}{1-p} k_0 \cdot \exp\left(-\frac{81,100}{RT}\right) P_{O_2}^{0.8} (1-X) \cdot \sqrt{1-5\ln(1-X)}$
[20]	Wire mesh, 850 °C Pine (P) Oak (O) Eucalyptus (E) Almond shell (AS) Olive stone (OS)	TGA 300–550	100–200	Air	P: $\frac{dX}{dt} = 3.8 \cdot 10^7 \cdot \exp\left(-\frac{140,000}{RT}\right) (1-X)^{0.4}$ O: $\frac{dX}{dt} = 4.3 \cdot 10^7 \cdot \exp\left(-\frac{136,000}{RT}\right) (1-X)^{1.1}$ E: $\frac{dX}{dt} = 9.2 \cdot 10^6 \cdot \exp\left(-\frac{142,000}{RT}\right) (1-X)^{0.9}$ AS: $\frac{dX}{dt} = 5 \cdot 10^7 \cdot \exp\left(-\frac{142,000}{RT}\right) (1-X)^{1.1}$ OS: $\frac{dX}{dt} = 3 \cdot 10^7 \cdot \exp\left(-\frac{134,000}{RT}\right) (1-X)$
[21]	Pine wood Screen heater reactor 600 °C, 300 °C/s	TGA Packed bed 300–450	80–106	2.25–36	$\frac{dX}{dt} = 5.3 \cdot 10^5 \cdot \exp\left(-\frac{125,000}{RT}\right) P_{O_2}^{0.53} (1-X)^{0.49}$

temperature (K). $f(X)$ is the reaction model also known as the structure function. $h(P_{O_{2,s}})$ is the oxygen partial pressure function which represents the effect of oxygen partial pressure on the reaction rate. $k(T_p)$ is the temperature dependent rate constant which is described by the Arrhenius equation:

$$k(T_p) = A \cdot \exp\left(-\frac{E_a}{RT_p}\right) \quad (2)$$

where A is the pre-exponential factor, E_a is the activation energy ($J \cdot mol^{-1}$), R is the gas constant ($J \cdot mol^{-1} \cdot K^{-1}$). The oxygen partial pressure function can be given in the form of a power law:

$$h(P_{O_{2,s}}) = P_{O_{2,s}}^n \quad (3)$$

where n is the reaction order with respect to oxygen.

In the literature, most of the authors employed Eqs. (1)–(3) to represent the kinetic of biomass char combustion [33]. However, some researchers [34,35] have used a Langmuir-Hinshelwood formulation which describes the competition between adsorption and desorption phenomena on the char surface. It provides a description of the O₂ adsorption and CO (CO₂) desorption process during carbon oxidation from the writing of elementary reaction steps [30,36]. The simplest Langmuir-Hinshelwood formulation is expressed as follow:

$$k(T_p) \cdot h(P_{O_{2,s}}) = R_{global} = \frac{k_d k_a P_{O_{2,s}}}{k_a P_{O_{2,s}} + k_d} \quad (4)$$

where k_d and k_a are the rate constants for desorption and adsorption process respectively and follow an Arrhenius law.

The Langmuir-Hinshelwood formulation predicts an effective reaction rate which varies with oxygen partial pressure and temperature. This form exhibits the two following limiting cases at a given pressure: when the adsorption process is the limiting step then $R_{global} = k_a P_{O_{2,s}}$ (first order of Eq. (3)) and when the desorption process is the limiting step then $R_{global} = k_d$ (zeroth order of Eq. (3)). According to Hurt and Calo [30], measured activation energies for desorption are in the range of 160–400 kJ/mol. These last values are much greater than those for adsorption which are comprised between 10 and 125 kJ/mol.

The structure function $f(X)$ represents the reactive surface of the particle. Its evolution during the gasification or combustion reactions is difficult to predict and is subject to discussion in the literature [14]. Due to the complex char structure, several kinetic models are reported in the literature to represent the structure

function. According to Tables 1 and 2, the most commonly used models for char combustion are the Power Law Model (PL) and the Volumetric Model (VM) [37]. The Power Law Model is totally empiric in nature while the Volumetric Model assumes a homogeneous reaction throughout the particle. In the case of char gasification with carbon dioxide or steam, the Shrinking Core Model (SCM) [38] is also frequently used to represent kinetic data [39,40]. These three models (i.e. PL, VM and SCM) describe a decrease in reaction rate with conversion. Finally, the Random Pore Model (RPM) proposed by Bathia et al. [41] has received much interest due to its ability to predict a maximum reaction rate which is often observed during combustion and gasification of char. This model introduces a structural parameter by considering that the char particle is porous and the reaction occurs at the internal surface of the pores. As the reaction proceeds, a random overlapping of the pores occurs which can increase or reduce the reactive surface area. This model was largely used for gasification of char with CO₂ and steam [39]. A very few authors [17,19] also found that the Random Pore Model satisfactorily fitted the reaction rate of biomass char combustion. In some cases, some authors [42] represented the structure function with a 6th order polynomial function which is totally empiric in nature.

As it can be observed in Tables 1 and 2, the majority of researchers [22–25,28,43] considers a global kinetic model for char combustion with activation energies ranging between 70,500 and 182,600 J/mol and reaction orders with respect to oxygen between 0.53 and 0.85. According to Di Blasi [33], this dispersion in the kinetic parameters is caused by different biomasses and char properties, pyrolysis conditions, amount and composition of ash, operating conditions and device of the experiments. It is important to note that several authors [20,22,28] incorporated the dependence of reactivity on the oxygen partial pressure into the pre-exponential factor so that the results are only valid for the gaseous mixture (air) used in the experiments [33].

However, some authors [17,44] have reported two zones on the curve of conversion rate versus temperature during non-isothermal combustion: a shoulder at low temperatures followed by a sharp peak. They attributed these two peaks to two phenomena which occur in parallel, a devolatilization step and a combustion step. During the kinetic study of beech char combustion, Branca et al. [44] concluded that a two-steps reaction mechanism which takes into account both devolatilization and combustion reactions provides a good description of measured data. According to these authors, the devolatilization stage is well described by a

relatively low activation energy compared to the one of char combustion [17,44].

In the literature, isothermal combustion of char in TGA is achieved by employing a switching gas method [19,21]. It consists in heating the reactor under an inert atmosphere to the desired reaction temperature before switching the gas from inert to reactive to perform the combustion. This technique is also employed for isothermal char gasification with H₂O [45] or CO₂ [18,39] in TGA. After the switching gas method, the newly introduced agent has to diffuse and replace the former gas in the apparatus. It is known that the time necessary for totally replacing the inert gas is likely to affect the char combustion rate [46] as it would cause a continuous change in the oxygen concentration or partial pressure in the TGA. For example, Zeng et al. [47] mentioned that it required 5–10 min for the TGA to reach a steady state after switching the gas from N₂ to CO₂. Therefore, it appears essential to take into account the variation of oxygen partial pressure in the TGA for determining the kinetic of char combustion.

The aim of the present study is to determine the combustion kinetic of biomass char in isothermal conditions. This char was obtained by fast pyrolysis of beech bark pellet in a fluidized bed reactor and thoroughly characterized in a previous paper to understand its physicochemical properties and reactivity [9].

This article is divided into two parts:

1) The first part of this paper focuses on the production of char and the determination of its physicochemical properties. The TGA protocol is defined and the TGA response time just after switching the gas from inert to reactive is investigated. The purpose is to observe and to model the evolution of oxygen partial pressure as it directly influences the kinetic of char combustion.

2) The second part of this article is the kinetic determination of isothermal char combustion in TGA. Experiments are carried out at atmospheric pressure and various temperatures ranging from 330 to 850 °C and oxygen partial pressures ranging from 5065 to 21,273 Pa. The response time of the TGA is integrated in the kinetic modelling so that the variation in the oxygen partial pressure is taken into consideration. Several kinetic models are tested and the most appropriate one is selected to represent the combustion reactivity of char in Regime I. Finally, the influence of mass transfer phenomena in the TGA is investigated.

2. Experimental section

2.1. Char preparation

The biomass used in this work is cylindrical pellets of beech bark (D = 6 mm, L = 15 mm) obtained by mechanical compaction

of sawdust. A picture of the raw material is given in Fig. 1(A). The proximate analysis of the biomass was carried out following the standard test method for chemical analysis of wood charcoal D 1762-84. The results are given in Table 3. The apparent density of the biomass was measured from the weight and volume of five single particles and is equal to $1050 \pm 11 \text{ kg/m}^3$.

Fast pyrolysis of the biomass was carried out under an inert atmosphere of nitrogen by instant immersion of a fixed mass of biomass particles in a batch dense fluidized bed reactor containing 5 kg of sand particles. The experimental details have been given elsewhere [9]. Briefly, the reactor consists of a refractory steel tube with 125 mm inner diameter and 1110 mm height equipped with a perforated plate distributor. It is surrounded by two electric furnaces delivering 6 kW electric powers. The fluidizing gas flow rate is measured by a rotameter before feeding the bed. A cyclone and a condenser collect respectively the elutriated particles and condensable vapors at the outlet of the reactor. The biomass injection system is made of a cylindrical tube of 25 mm diameter with the lower end located inside the fluidized bed. An injected biomass mass of 20 g was chosen to prevent a temperature decrease superior to 5 °C.

The experiments are carried out with a fixed nitrogen mass flow rate of 7 kg/h, corresponding to 7 times the minimum fluidization velocity of sand at 850 °C.

The fast pyrolysis of the beech bark pellet was performed at 850 °C and at atmospheric pressure. This temperature was chosen since 850 °C is the operating condition of the gasifier in FICFB process. After reaching the pyrolysis temperature, about 20 grams of biomass are introduced inside the fluidized bed and the operation is repeated at least 5 times to produce a significant amount of chars. After the pyrolysis, the produced chars are cooled under a flow of nitrogen before being recovered the day after by sieving. A picture of the obtained chars is given in Fig. 1(B). The soaking time at bed temperature was approximately 3 h. The produced char was stored inside a pill-box until it was analyzed. The apparent density of char particles just after the pyrolysis process is equal to $333 \pm 24 \text{ kg/m}^3$.

The physical and chemical properties of the biomass and its associated char are summarized in Table 4. True density was obtained by helium pycnometer.

2.2. Mercury porosimetry analysis

Char particles obtained from fast pyrolysis of biomass are known to be porous particles containing numerous pores. These pores are usually classified as micropores ($d_{\text{pore}} < 2 \text{ nm}$), mesopores ($2 \text{ nm} < d_{\text{pore}} < 50 \text{ nm}$) and macropores ($d_{\text{pore}} > 50 \text{ nm}$). Mercury porosimetry analysis enables to quantify the volume of pores larger than 3 nm by injecting mercury into the grinded chars under

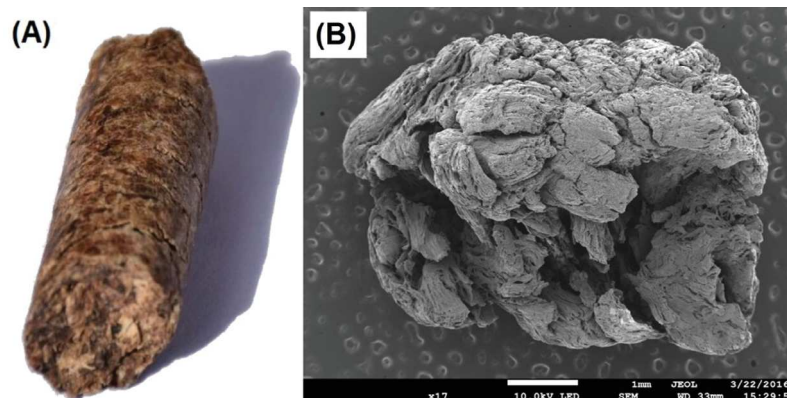


Fig. 1. Picture of the (A) beech bark pellet (PEL) and (B) its associated char (PEL850) obtained by pyrolysis at 850 °C in fluidized bed reactor.

Table 3

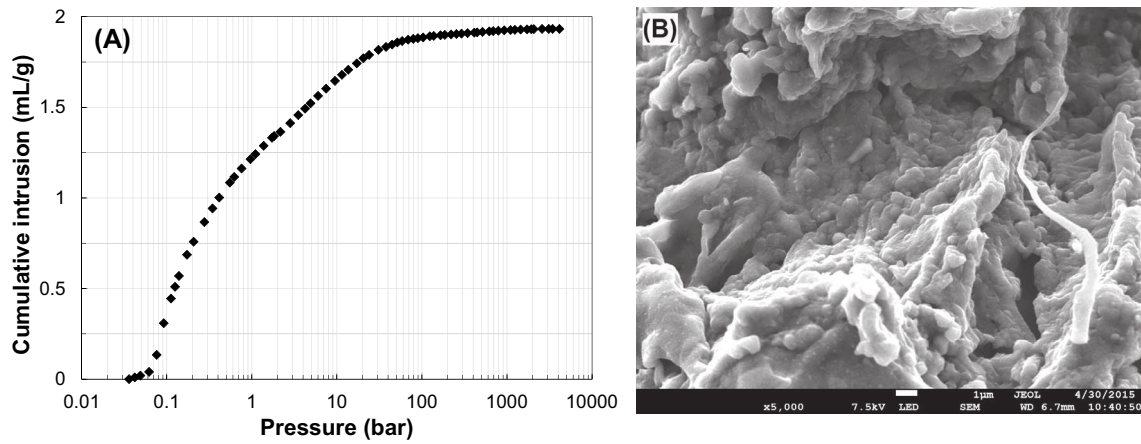
Proximate analysis of the beech bark pellet (wt%, dry basis).

Biomass	Moisture (%)	Volatile matters (%)	Fixed carbon ^a (%)	Ash (%)
Beech bark pellet	10.9	75.13	11.15	2.82

^a by difference.**Table 4**

Ultimate analysis and physicochemical properties of the produced char.

Material	Pyrolysis conditions Pyrolysis Temp. (°C)	True density $\rho_{t,c}$ (kg/m ³) He pycnometer	Ultimate analysis (db, wt%)				Chemical Formula
			C	H	O	Ash	
PEL	-	1433.3	44.79	6.09	47.29	2.82	CH _{1.63} O _{0.79}
PEL850	850	1832.5	75.49	0.56	6.06	17.89	CH _{0.09} O _{0.06}

**Fig. 2.** (A) Cumulative pore volume versus pressure from mercury porosimetry analysis of PEL850, (B) SEM picture of grinded char particle.**Table 5**

Physicochemical properties of the grinded char particles, results from mercury porosimetry analysis.

Char	Apparent density ρ_a (kg/m ³)	True density (kg/m ³)	Mean pore diameter d_{pore} (nm)	Porosity ε_p (%)	Porosity of meso and macropores (%)	Surface area (m ² /g)
PEL850	827	1585.7	723	55	13	10.7

increasing pressure from 0 to 4000 bars. This analysis was carried out on PEL850 with an AUTOPORE IV apparatus from Micromeritics. Prior to this analysis, the char was grinded to ensure that all particles have approximately the same diameter (sauter diameter equal to 25 μm). Fig. 2(A) presents the results of the cumulative intrusion volume versus pressure. For pressure equal to 2 bars, the cumulative intrusion volume corresponds to the filling of interstitial area between the grinded char particles. From this result, the apparent density ρ_a of grinded char particles can be calculated and is equal to 827 kg/m³. For pressures above 2 bars, the cumulative intrusion volume represents the filling of pores with a diameter greater than 3 nm. As mentioned by several authors [14], one of the main problems of mercury porosimetry analysis is that char structure might be broken during the increase of pressure. Therefore, results reported may be affected by a large degree of uncertainty. Results of mercury porosimetry are given in Table 5. The true density given in this table takes into account both macro- and mesopores and does not consider the presence of micropores. The porosity ε_p of grinded char particles is calculated from Eq. (5) and is equal to 55%. From the value of the true density given in Table 5, the porosity related to macro- and mesopores can be calculated and is equal to 13%.

$$\varepsilon_p = 1 - \frac{\rho_a}{\rho_{t,c}} \quad (5)$$

Physical nitrogen adsorption at 77 K was also carried out in order to determine the total char surface area. During this experiment, nitrogen diffusion was very slow and we could not obtain exploitable results. It is well-known in the literature that nitrogen cannot penetrate deeply into micropores and sometimes equilibrium cannot be achieved in such experiments [7]. This indicates that PEL850 contains some micropores. Nevertheless, as oxygen molecules have similar molecular diameter compared to the one of nitrogen molecules, the presence of micropores in the char does not influence the combustion kinetic since oxygen molecules cannot diffuse inside.

SEM picture of grinded particles of PEL850 is presented in Fig. 2 (B) and showed that this char is composed of elementary very fine char grains with a diameter less than 1 μm . Besides, mercury porosimetry revealed that the average pores diameter is equal to 723 nm. This average pores diameter can be considered as a hydraulic diameter in which the oxygen diffuses toward the elementary grains. This hydraulic diameter represents the interstitial space of an agglomeration of elementary grains with a diameter d_g .

The elementary grain diameter is then calculated according to the following expression:

$$d_g = \frac{6}{4} \cdot \frac{\varepsilon_p}{1 - \varepsilon_p} d_{pore} \quad (6)$$

where d_g is the elementary char grain diameter (m), ε_p is the porosity of the grinded char particles and d_{pore} is the average pore diameter of the grinded char particles (m).

From Eq. (6), the elementary char grain diameter was found to be equal to 0.9 μm which is in good agreement with results observed in Fig. 2(B). Hence, it can be assumed that the elementary grains are made of micropores which are not accessible for oxygen molecules.

2.3. Isothermal TGA combustion tests

2.3.1. TGA protocol

Char reactivity in combustion was measured using isothermal TGA analyses with a TGA Q600 analyzer from TA Instruments. The grinded particles with a sauter diameter of 25 μm are used. Preliminary, tests with various sample weights ranging from 2 to 15 mg confirmed that 8–10 mg is the optimum sample weight which enables to achieve accurate and repeatable results. Consequently, about 8 mg of PEL850 were introduced inside an alumina crucible (inner diameter and height of the crucible equal to 5.5 mm and 4 mm, respectively) for each test. The height of the char layer is $\delta_c = 0.7$ mm. The experimental protocol is divided into two stages. The first one, carried out under high-purity nitrogen flow (100 NmL/min), consists in:

- an initial period of 15 min at ambient temperature used to initialize the system,
- a linear heating rate of 10 $^{\circ}\text{C}/\text{min}$ from ambient temperature to the combustion temperature,
- a period of 15 min at the combustion temperature to stabilize the system.

The second stage is the isothermal combustion of char carried out by switching nitrogen to a mixture of N_2/O_2 with the same flow rate. Temperatures in the range of 330 to 450 $^{\circ}\text{C}$ were tested and a final analysis was carried out at a temperature of 850 $^{\circ}\text{C}$. Oxygen partial pressure was varied between 5065 and 12,273 Pa. All of the gas mixtures of N_2/O_2 were purchased from Air Liquide and have an accuracy of 0.1%.

During the first stage carried out under pure nitrogen, a mass loss less than 5% was observed for each experiment and combustion temperature up to 450 $^{\circ}\text{C}$. Klinghoffer et al. [48] reported similar mass losses in the char when heated under nitrogen in TGA. They attributed this mass loss to several phenomena:

- Water loss due to the presence of adsorbed water in the char pores since the char was stored at atmospheric conditions.
- The loss of volatile products which are still present in the char.

The conversion rate is calculated via the following equation:

$$X = \frac{w_i - w(t)}{w_i - w_{ash}} \quad (7)$$

where w_i , $w(t)$ and w_{ash} are the initial, temporal and final sample weight, respectively.

The apparent reaction rate was defined as the derivative of the evolution of the conversion rate versus time, for a conversion rate of 50%:

$$R_{app} = \left. \frac{dX}{dt} \right|_{X=0.5} \quad (8)$$

2.3.2. Response of the TGA to a concentration step

The purpose of this section is to observe the time necessary to the reactive gas to completely replace the inert gas just after switching the gas from inert to reactive. As mentioned by some authors, this time interval depends on the reactor geometry, the reactor volume and gas flow rate [49]. In our case, inner diameter and length of the cylindrical TGA furnace are respectively 22.86 mm and 174 mm. This study was carried out by connecting a paramagnetic gas analyzer SERVOMEX to the outlet of the TGA. This apparatus provides high performance oxygen monitoring and enables oxygen quantification after switching the gas from N_2 to a mixture of N_2/O_2 . Before entering the analyzer, the gas line is cooled into a gas cooler. The response time of the sampling gas lines and analyzer to an oxygen concentration step is given in Fig. 3. It consists in a pure delay of 1 min followed by a substantial increase of the oxygen fraction which can be considered as a concentration step.

To examine the time necessary to completely replace the inert gas by the reactive gas in the TGA after the switching gas method, blank experiments without char in the crucible were performed at three different temperatures (330, 500 and 850 $^{\circ}\text{C}$). They consist in heating the TGA in inert atmosphere to the run temperature, a period of 15 min at the run temperature and then switching the gas from N_2 to air. The switching method is considered as a concentration step and the oxygen molar fraction is continuously measured at the outlet of the TGA. The result of the temporal variation of the normalized oxygen fraction during an experiment at 500 $^{\circ}\text{C}$ is given in Fig. 3. Other experiments at 330 and 850 $^{\circ}\text{C}$ showed that the oxygen fraction profile is independent of the TGA temperature.

It can be seen that the response of the TGA to a concentration step can be divided into two parts:

- A pure delay for approximately two minutes which is associated with the response of a plug flow tubular reactor. During this period, the partial pressure of oxygen is equal to zero.
- A continuous increase of the oxygen fraction to a constant value. This profile is attributed to the behavior of a continuous flow stirred-tank reactor and represents the evolution of oxygen partial pressure around the crucible.

Consequently, during our isothermal char combustion experiments in thermogravimetric analyzer, it takes about 25 min for the mixture of N_2/O_2 to completely replace the inert gas in the apparatus after the switching gas method. Oxygen partial pressure

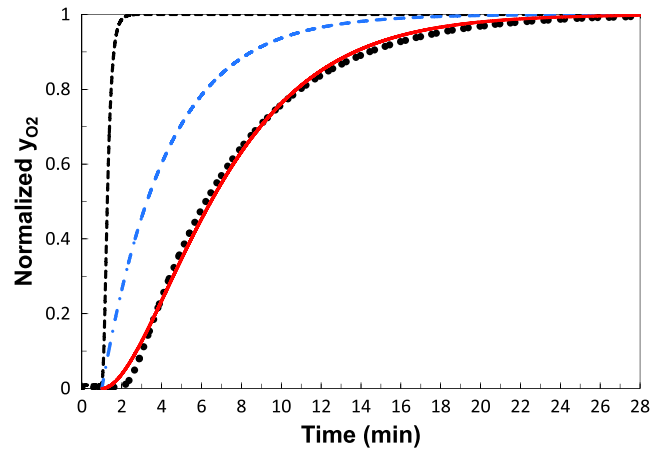


Fig. 3. TGA response time at 500 $^{\circ}\text{C}$. (---) Oxygen molar fraction of the sampling gas lines and analyzer, (••) Oxygen molar fraction at the TGA outlet, (---) and (—) oxygen molar fractions at the outlet of the continuous flow stirred-tank reactors 1 and 2, respectively.

can no longer be considered as constant during the initial part of char combustion. In the following, the pure delay of 1 min due to the gas sampling and analyzer was removed. In order to take into consideration this effect for determining char combustion kinetics, we chose to represent the transfer function of the TGA by the association of “n” continuous flow stirred-tank reactors in series with the same residence time according to the following differential equations system:

$$\begin{cases} \frac{dY_{O_2}^1}{dt} = \frac{1}{\tau_{CSTR}} \cdot (Y_{O_2}^{in} - Y_{O_2}^1) \\ \frac{dY_{O_2}^2}{dt} = \frac{1}{\tau_{CSTR}} \cdot (Y_{O_2}^1 - Y_{O_2}^2) \\ \vdots \\ \frac{dY_{O_2}^n}{dt} = \frac{1}{\tau_{CSTR}} \cdot (Y_{O_2}^{n-1} - Y_{O_2}^n) \end{cases} \quad (9)$$

where Y_{O_2} is the normalized molar fraction of oxygen which represents the measured oxygen percentage divided by the maximum oxygen percentage, $Y_{O_2}^{in}$ is the normalized molar fraction of oxygen at the inlet of the TGA ($Y_{O_2}^{in} = 1$), $Y_{O_2}^1 \dots Y_{O_2}^n$ are the normalized molar fractions of oxygen at the continuous flow stirred-tank reactors outlet 1...n respectively and τ_{CSTR} is the residence time of the continuous flow stirred-tank reactors.

The parameters n and τ_{CSTR} are identified by solving Eq. (9) using an explicit Runge Kutta (4,5) formula and applying the nonlinear least-squares curve fitting problem. Hence, the parameters n and τ_{CSTR} were found to be 2 and 3.3 min respectively. Fig. 3 presents the corresponding transfer function by taking two continuous flow stirred-tank reactors with a residence time of 3.3 min each. The model well represents experimental results. Therefore, in the following, the response time of the TGA will be taken into account for modelling the oxygen partial pressure in the kinetic expression (Eq. (1)).

2.3.3. Mass transfer within the crucible

The aim of this part is to evaluate the diffusional effects of oxygen which take place around and within the crucible. Indeed, during char combustion in TGA, a boundary layer is formed at the upper surface of the crucible. In this zone, the transfer of oxygen proceeds through convection. Besides, some authors [50–52] observed the presence of a stagnant gas region between the upper surface of the crucible and the surface of char particles. In this region, the oxygen may transfer through diffusion. These two diffusional effects can lead to significant gradients of oxygen concentration which decrease char reactivity in combustion.

Diffusional effects inside the crucible were estimated by vaporizing a small amount of about 15 mg of fine naphthalene ($C_{10}H_8$) particles at 110 °C in isothermal conditions. After loading about 15 mg of naphthalene particles in an alumina crucible (height of the naphthalene layer equal to 1 mm), the TGA was heated up with a linear heating rate of 50 °C/min up to 110 °C under high purity flow of nitrogen. A period of 1 h at 110 °C was maintained to totally vaporize naphthalene. From the recorded mass loss, naphthalene evaporating mass flow rate was calculated and plotted versus time for different nitrogen volume flow rates (i.e. 50, 100 and 150 NL/min) in the TGA. It was observed that naphthalene vaporization mass flow rate substantially increases (during the non-isothermal period) before reaching a constant value. Besides, this mass flow rate was found to be independent of the nitrogen volume flow rate. This indicates that transfer resistance through convection is negligible compared to transfer resistance through diffusion inside the crucible. From the constant naphthalene mass flow rate, the global mass transfer coefficient is determined and is equal to $3.67 \cdot 10^{-3}$ m/s. This value is very close to the term $D_{C_{10}H_8-Air} / (H - \delta_{C_{10}H_8})$ which corresponds to the diffusion of naph-

thalene through the stagnant zone in the crucible. $D_{C_{10}H_8-Air}$ represents the diffusion coefficient of naphthalene into air (m^2/s). This coefficient is dependent on the temperature and is calculated from ref [53].

Therefore, during naphthalene vaporization in TGA, mass transfers mainly occur through diffusion inside the stagnant zone in the crucible. Besides, naphthalene transfer through convection at the upper surface of the crucible is not the limiting step and can be neglected compared to naphthalene diffusion.

Consequently, during char combustion in TGA, oxygen mass transfers around and within the crucible can be modelled by pure diffusion phenomena of oxygen into N_2 in the stagnant zone.

3. Results and discussion

3.1. Effect of combustion temperature

Fig. 4 presents the effect of combustion temperature on the conversion rate and the sample temperature profile during the combustion of PEL850 in the TGA.

First, it can be seen that the conversion rate is highly dependent on the combustion temperature, especially for temperatures up to 400 °C. This result is well-established in the literature for both combustion and gasification of char [39]. For instance, at a given conversion rate of 0.5, it requires a much shorter reaction time at a higher combustion temperature (181 min, 84.5 min, 43.0 min, 31.8 min, 18.8 min for temperatures of 330 °C, 350 °C, 370 °C, 380 °C and 400 °C respectively). For higher temperatures, this effect is less significant and the reactivity is very high. It takes 8.8 min and 5.6 min for temperatures of 450 °C and 850 °C respectively. Fig. 4(A) also shows that a pure delay is noticed at the beginning of the reaction. Indeed, the conversion rate is equal to zero for approximately 1 min before gradually increasing. This can be explained by the response time of the TGA (see Section 2.3.2). During this pure delay of 1 min, the oxygen partial pressure is null and the combustion has not begun. The steady state of oxygen partial pressure is obtained 25 min after the switching gas method. Consequently, the combustion is strongly impacted by the TGA response time.

Fig. 4(B) reports the sample temperature profile in the TGA during the combustion. For each experiment, the sample temperature first substantially increases before gradually decreasing to the pre-set combustion temperature. For temperatures up to 400 °C, the temperature raise is less than 5 °C. Consequently, the combustion can be considered as isotherm in this range of temperatures. Nevertheless, above 400 °C, the strong exothermicity of the combustion leads to a significant increase in the sample temperature (about 20 °C at 450 °C) and a faster reaction. The combustion is no longer isotherm. Therefore, in the following, the kinetic study is performed in isothermal conditions for temperatures up to 400 °C.

Intrinsic reactivity and kinetic of char combustion correspond to the intrinsic chemical transformations which occur when the chemical reaction is the limiting step compared to external mass and heat transfers. Hence, the oxidative reaction must occur in Regime I [8]. Fig. 5 shows the logarithm of the apparent reaction rate (Eq. (8)) versus $1/T$ for the combustion of PEL850 under a constant partial pressure of oxygen (21,273 Pa). The reaction of combustion can be divided into three main regimes. Regime I occurs for temperatures up to 400 °C. Considering Eqs. (1)–(3) and from the slope of the straight line, it is possible to determine activation energy without considering any reaction models. Its value is equal to 125 kJ/mol. However, this method is still subject to discussions as activation energy may be dependent on the level of conversion [31,54]. Activation energy found in Regime I is considered as the

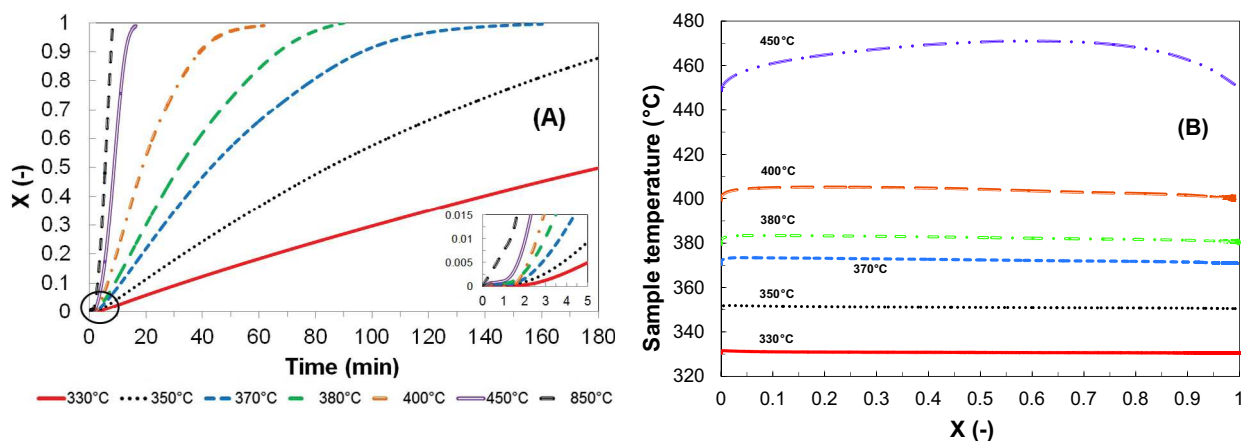


Fig. 4. (A) Conversion rate versus time, (B) Sample temperature versus conversion rate, (effect of temperature – $P_{O_2} = 21,273$ Pa).

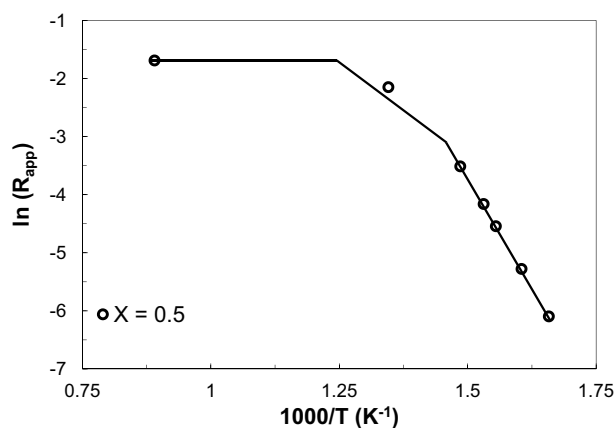


Fig. 5. Logarithm of the apparent reaction rate versus $1/T$ at a given conversion rate of 0.5 during the combustion of PEL850 in TGA in air.

intrinsic activation energy of char combustion. Regime II takes place for temperatures between 450 and 600 °C. In this regime, the apparent activation energy is much lower compared to the one obtained in Regime I. Finally, Regime III arises for higher temperatures and is associated with an apparent activation energy close to zero [8].

It is important to note that, in the case of char combustion with air in FICFB process, the reactor operates at 950 °C. According to Fig. 5, the combustion should occur in Regime III. However, the oxygen partial pressure in the reactor is much lower than 0.21 bar because of oxygen consumption and carbon dioxide production during the char combustion. Hence, a low value of the oxygen partial pressure strongly decreases the char reactivity and the chemical reaction cannot be considered as negligible compared to external mass transfers. Therefore, in these types of reactor, it is necessary to take into account both mass transfers and intrinsic kinetic of char combustion. This is why, in this work, determination of intrinsic kinetic is carried out in Regime I. This occurs for temperatures up to 400 °C.

3.2. Effect of oxygen partial pressure

The influence of oxygen partial pressure was performed at 400 °C and the results are shown in Fig. 6. A raise of the oxygen partial pressure leads to a higher combustion rate. A short delay at the beginning of the reaction can still be observed in Fig. 6(A) indicating that the effect of the TGA response time is still present

for various oxygen partial pressures. Again, considering Eqs. (1)–(3) and from the slope of the straight line of Fig. 6(B), it is possible to determine the reaction order with respect to oxygen. Its value is equal to 0.67.

3.3. Combustion rate profile

Fig. 7 illustrates the effect of temperature and oxygen partial pressure on the combustion rate profile during the isothermal combustion of PEL850 in TGA in Regime I. It can be seen that, for each experiment, the combustion rate first increases before reaching a maximum value followed by a gradual decrease. This maximum is frequently observed during char gasification [46,47,49,55] and combustion [19,21]. Two different points of view can be found in the literature. First, some authors [49,55,19,21] attributed the maximum reaction rate to a change of the char reactive surface during the reaction. Hence, they attempted to represent the reaction rate profile using the Random Pore Model proposed by Bathia et al. [41]. In this model, the change of pore surface area of the particle during the reaction can explain the existence of a maximum combustion rate. Indeed, an increase in the combustion rate is due to the growth of pores surface area while a decrease is attributed to the coalescence of neighboring pores. A maximum combustion rate occurs when the second effect overshadows the first effect. Finally, the second point of view is that the maximum reaction rate is due to the low gasification agent content in the reactive atmosphere just after switching the gas from inert to reactive. For instance, in the case of CO₂ and steam gasification of coal char, some researchers [46,47,49] concluded that the time necessary to reach a maximum reaction rate is independent of the type and partial pressure of the gasifying agent for a constant gas flow rate in the TGA. This time is then related to a dispersion phenomenon and is not associated with changes on the char surface during gasification [46].

A slow increase in the combustion rate is also observed in Fig. 7. This phenomenon occurs at a conversion of about 0.7 for every combustion temperatures and oxygen partial pressures. According to Table 4, PEL850 contains a large amount of ash which is composed of 39% of silica, 40% of calcium, 2% of sodium, 12% of potassium and 7% of magnesium. The significant ash content can lead to a catalytic effect during char combustion. Therefore, the slow increase of the combustion rate observed for conversion above 0.7 can be associated with the catalytic effect of ash.

In the literature, several kinetic models were used to represent the kinetic of char combustion. They have been presented in the introduction. Among them, the Power Law Model, the Volumetric

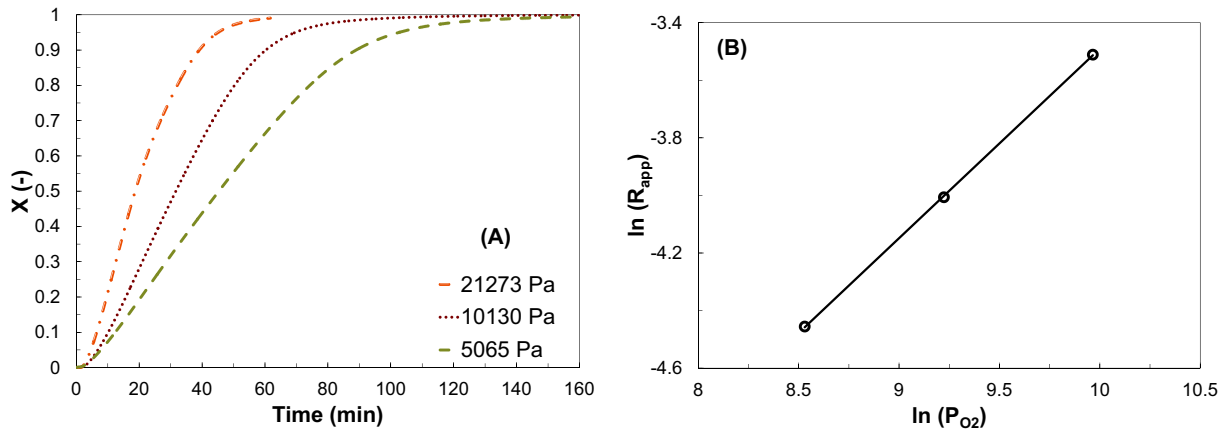


Fig. 6. (A) Conversion rate versus time, (B) logarithm of apparent reaction rate versus logarithm of oxygen partial pressure, (effect of oxygen partial pressure – $T = 400\text{ }^{\circ}\text{C}$).

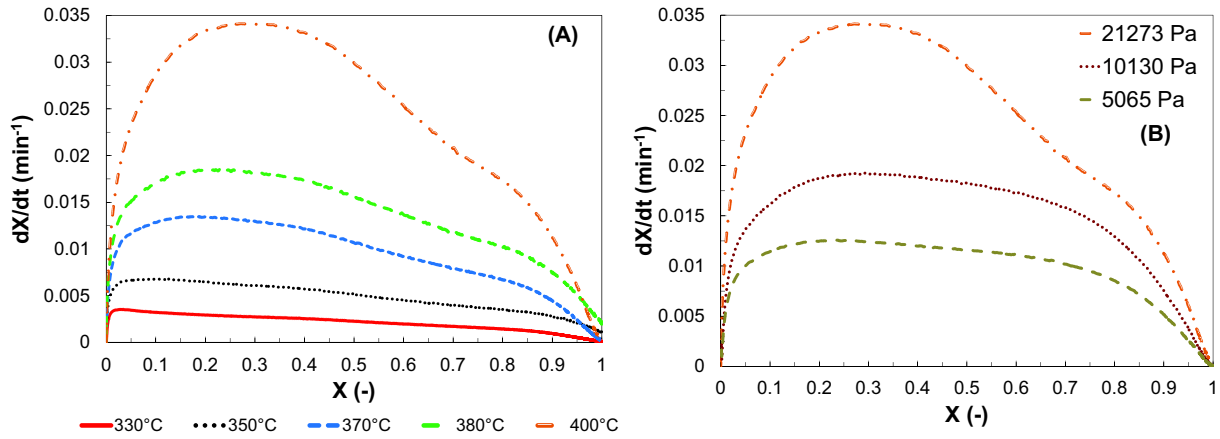


Fig. 7. Combustion rate versus conversion rate: (A) effect of combustion temperature ($P_{O_2} = 21,273\text{ Pa}$), (B) effect of oxygen partial pressure at $400\text{ }^{\circ}\text{C}$.

Model and the Shrinking Core Model are classified into deceleratory models which represent a decrease of the combustion rate versus conversion. Other models such as the Avrami-Erofeyev (A) Models [32] can be found which are based on nucleation and nuclei growth models. These last models as well as the Random Pore Model are known as sigmoidal models which show a bell-shaped relationship between reaction rate and conversion rate [32]. These models are able to predict a maximum combustion rate and according to the shape of the curve in Fig. 7 may have much interest to represent kinetic of char combustion.

3.4. Kinetic modelling

3.4.1. Kinetic models

In this work, a large amount of models were tested (i.e. PL, VM, SCM, RPM and Avrami-Erofeyev (A) Models). Two models were found to be in good agreement with experimental data: the Shrinking Core Model [38] and the Random Pore Model [41]. These two models are presented below.

The SCM [38] assumes that the reaction takes place at the outside surface of a non-porous particle with an initial radius R_0 in isothermal conditions. As the reaction proceeds, the surface moves into the interior of the solid leaving behind an inert ash. By considering a spherical particle and a pseudo-steady-state regime, the reaction rate can be expressed as:

$$\frac{dX}{dt} = \frac{S_{p0}M_c}{\rho_{t,c}(1-\varepsilon_p)x_c} A_{GM} \cdot \exp\left(-\frac{E_a}{RT_p}\right) \cdot P_{O_2,i}^n \cdot (1-X)^{2/3} \quad (10)$$

where S_{p0} is the external surface area of the initial char particles per unit volume (m^2/m^3), M_c is the molar weight of carbon ($\text{kg}\cdot\text{mol}^{-1}$), $\rho_{t,c}$ is the true density of the char ($\text{kg}\cdot\text{m}^{-3}$), x_c is the mass fraction of carbon in the char particle and A_{GM} is the pre-exponential factor ($\text{mol}\cdot\text{m}^{-2}\cdot\text{Pa}^{-n}\cdot\text{s}^{-1}$).

In the case of a spherical porous char particle, each particle is considered as made up of a large number of non-porous spherical grains of uniform radius r_g . It is then assumed that the reaction of each grain proceeds from the outside toward the center so that the reaction front within each grain exhibits spherical symmetry [8]. Hence, Eq. (10) obtained for a reaction of a non-porous char particle applies directly to the individual grain and is called the Grain Model (GM) [8]. Hence, the difference between the SCM and the Grain Model arises from the expression of the external surface area. In our case, we showed that PEL850 is a porous char particle made of numerous non-porous grains. Hence, the Grain Model is used and the external surface area is expressed as:

$$S_{p0} = \frac{3}{r_g} \quad \text{for the Grain Model} \quad (11)$$

where $r_g = 0.45\text{ }\mu\text{m}$. The value of S_{p0} is equal to $6.66\cdot 10^6\text{ m}^2\cdot\text{m}^{-3}$. To determine kinetic parameters (i.e. pre-exponential factor, activation energy and reaction order with respect to oxygen), most of the authors [39] in the literature use a graphical resolution by integrating Eq. (10) and plotting the left hand side versus time:

$$1 - (1-X)^{1/3} = K_{GM} \cdot t \quad (12)$$

From the slope of the straight line (Eq. (12)), kinetic parameters can be determined for various combustion temperatures and oxygen partial pressures.

The RPM [41] was performed since the char is characterized by the presence of fine pores [9]. This model considers that the reaction takes place at the surface of the pores of a solid particle. As the reaction progresses, it is assumed that neighboring surface inside the particle will intersect one another and pores will overlap. By considering a spherical particle, the reaction rate is given by:

$$\frac{dX}{dt} = \frac{S_0}{1 - \varepsilon_p} A_{RPM} \cdot \exp\left(-\frac{E_a}{RT_p}\right) \cdot P_{O_{2,i}}^n \cdot (1 - X) \sqrt{1 - \varphi \ln(1 - X)} \quad (13)$$

where S_0 is the initial internal surface area per unit volume ($\text{m}^2 \cdot \text{m}^{-3}$), ε_p is the initial porosity of the particle, A_{RPM} is the pre-exponential factor ($\text{m}^3 \cdot \text{m}^{-2} \cdot \text{Pa}^{-n} \cdot \text{s}^{-1}$) and φ is a structural parameter related to the pore structure of the initial char. The value of φ can be expressed by the following equation:

$$\varphi = \frac{4\pi L_0(1 - \varepsilon_p)}{S_0^2} \quad (14)$$

where, L_0 is the initial pore length per unit volume ($\text{m} \cdot \text{m}^{-3}$). A value of φ equal to 0 represents the volumetric model while value of φ equal to 1 is close to the Shrinking Core Model [41]. Hence, a maximum reaction rate arises when the value of the parameter φ is large (above 2). Besides, the larger the value of φ , the more acute is the peak. In the literature, some authors [55] used a graphical approach to determine both the structural parameter φ and the kinetic parameters (K_0 , E_a and n) according to Eqs. (15) and (16).

$$\varphi = \frac{2}{2 \ln(1 - X_{max}) + 1} \quad (15)$$

where X_{max} is the conversion rate related to the maximum combustion rate. An integration of Eq. (13) gives the following relation [41]:

$$\frac{2}{\varphi} \cdot \left[\sqrt{1 - \varphi \ln(1 - X)} - 1 \right] = K_{RPM} \cdot t \quad (16)$$

A linear evolution of the left hand side of Eq. (16) versus time for different temperatures and oxygen partial pressures enables to determine the kinetic parameters from the slope of the line.

3.4.2. Modelling

The graphical method described above for the two models was not employed in this work since the oxygen partial pressure cannot be considered as uniform in the first 25 min of the char combustion. To obtain kinetic parameters, a differential equations system was defined which takes into consideration both the response time of the TGA and the intrinsic kinetic of char combustion (GM or RPM). It is given in the following expression:

$$\left\{ \begin{array}{l} \text{TGA Response Time} \left\{ \begin{array}{l} \frac{dP_{O_{2,1}}}{dt} = \frac{1}{\tau_{CSTR}} \cdot (P_{O_{2,in}} - P_{O_{2,1}}) \\ \frac{dP_{O_{2,2}}}{dt} = \frac{1}{\tau_{CSTR}} \cdot (P_{O_{2,1}} - P_{O_{2,2}}) \end{array} \right. \\ \text{Kinetic Models} \left\{ \begin{array}{l} \frac{dX}{dt} = \frac{S_{p0} M_c}{\rho_{t,c} (1 - \varepsilon_p) X_c} A_{GM} \cdot \exp\left(-\frac{E_a}{RT_p}\right) \cdot P_{O_{2,2}}^n \cdot (1 - X)^{2/3} \quad \text{for the GM} \\ \frac{dX}{dt} = \frac{S_0}{1 - \varepsilon_p} A_{RPM} \cdot \exp\left(-\frac{E_a}{RT_p}\right) \cdot P_{O_{2,2}}^n \cdot (1 - X) \sqrt{1 - \varphi \ln(1 - X)} \quad \text{for the RPM} \end{array} \right. \end{array} \right. \quad (17)$$

The kinetic parameters A_{GM} , A_{RPM} , E_a and n are estimated by solving Eq. (17) using an explicit Runge Kutta (4,5) formula and applying the nonlinear least-squares curve fitting problem. It con-

Table 6

Kinetic parameters obtained with the Grain Model by solving the differential equation system given in Eq. (17).

Char type	A_{GM} ($\text{mol} \cdot \text{m}^{-2} \cdot \text{Pa}^{-n} \cdot \text{s}^{-1}$)	E_a (J/mol)	n (-)	$\min_x \ f(x)\ _2^2$
PEL850	19.06	123,780	0.74	30.51

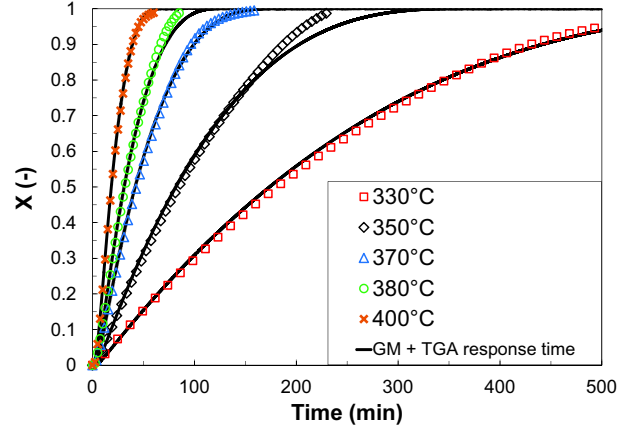


Fig. 8. Comparison between conversion rate obtained from char combustion in TGA and the conversion rate obtained from the Grain Model including the response time of the TGA.

sists in minimizing the sum of the difference between each experimental data and the one corresponding to the model for all temperatures and oxygen partial pressures according to the following expression:

$$\min_x \|f(x)\|_2^2 = \min_x \left(\sum_{i=1}^N f_i(x)^2 \right) \quad (18)$$

where $f_i(x) = X_{exp} - X_{mod}$, x represents the kinetic parameters and N corresponds to the number of experimental data.

In the case of the Grain Model, the values of pre-exponential factor, activation energy and reaction order with respect to oxygen are given in Table 6. It can be seen that activation energy is similar to that obtained in Section 3.1. Its value is also in good agreement with those obtained in the literature [33]. Likewise, reaction order with respect to oxygen is also in the same order of magnitude compared to some previous works (see Tables 1 and 2). Comparisons between experimental data and results obtained from the Grain Model including the response time of the TGA are given in Figs. 8 and 9. The intrinsic GM for a combustion temperature of 400 °C is also reported in Fig. 9. A very good agreement is found between experimental and predicted results. Fig. 9 shows that, taking into

account the non-uniform oxygen partial pressure in the initial stage of the combustion enables the GM to predict a maximum in the reaction rate.

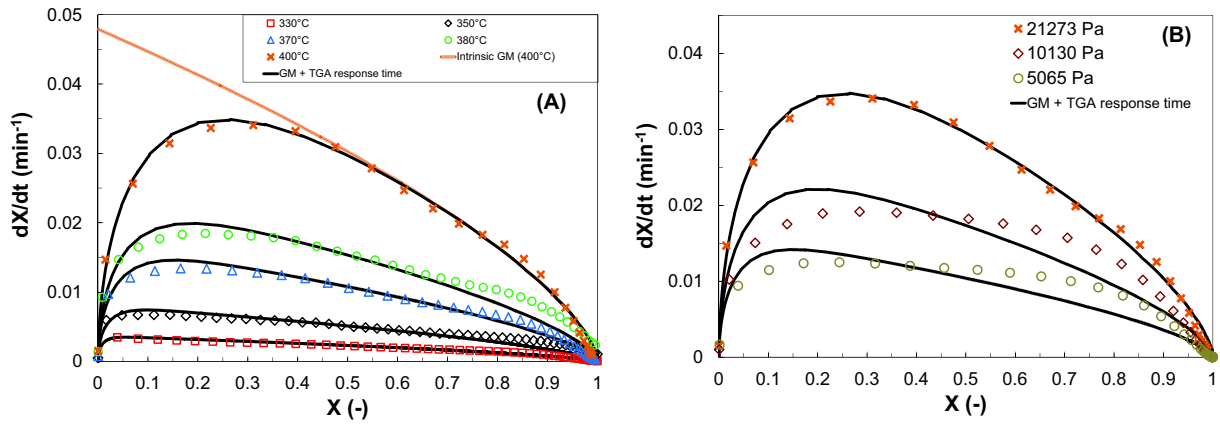


Fig. 9. Comparison between combustion rate obtained by isothermal combustion of PEL850 in TGA and the combustion rate from the GM including the response time of the TGA, (A) at various temperatures in air, (B) at different oxygen partial pressures at 400 °C.

Table 7

Kinetic parameters obtained with the Random Pore Model by solving the differential equations system given in Equation (17).

Char type	$K_0 = \frac{S_0}{1-\phi} A_{RPM}$ (Pa ⁿ .s ⁻¹)	E_a (J/mol)	n (-)	ϕ (-)	$\min_x \ f(x)\ _2^2$
PEL850	1638.13	123,140	0.72	2.9	19.90
PEL850	1992	124,040	0.74	1	47.47

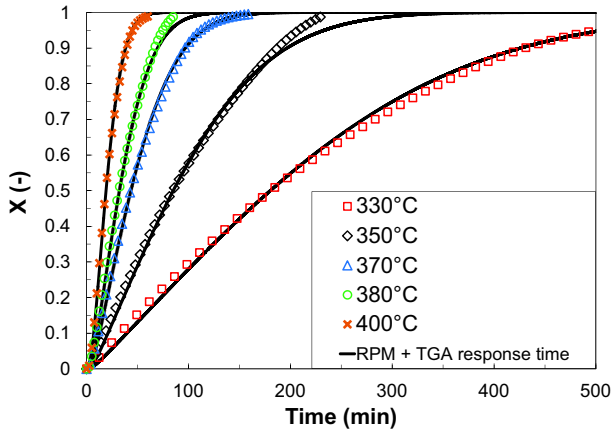


Fig. 10. Comparison between conversion rate obtained from char combustion in TGA and the conversion rate obtained from the Random Pore Model ($\phi = 2.9$) including the response time of the TGA.

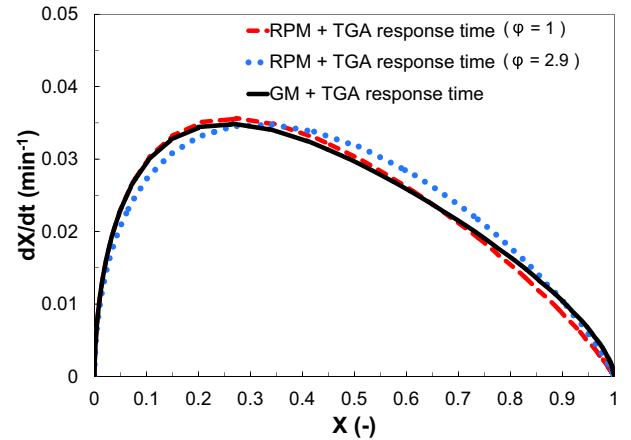


Fig. 11. Comparison between the Random Pore Model with values of $\phi = 2.9$ and 1 and the Grain Model including the response time of the TGA, combustion at 400 °C under air.

In the case of the Random Pore Model, the values of pre-exponential factor, activation energy, reaction order with respect to oxygen and structural parameter are given in Table 7. Comparisons between experimental data and results obtained from the Random Pore Model including the response time of the TGA are given in Fig. 10. The structural parameter is larger than 2 indicating that a maximum reaction rate arises during the char combustion. In the literature, several authors [17,19] mentioned that the Random Pore Model satisfactorily fitted the experimental combustion rate. During the isothermal combustion of lignin and three hardwoods, Magnaterra et al. [19] found a value of the structural parameter equal to 2.6 and 5 according to the type of chars, reaction orders with respect to oxygen in the range of 0.7–0.82 and activation energies between 78 and 128 kJ/mol. In the case of combustion of coal char in TGA, Kajitani et al. [56] concluded that the

ideal value of ϕ is 14, reaction order with respect to oxygen and activation energy were found to be equal to 130 kJ/mol and 0.68, respectively.

Table 7 also indicates the values of pre-exponential factor, activation energy and reaction order with respect to oxygen obtained for a constant value of ϕ equal to 1. As mentioned above, when ϕ is equal to 1, the structure functions of both the RPM and the GM are very close to each other. This result is highlighted in Fig. 11 which shows that combustion rate obtained with the GM is very close to the one obtained with the RPM with ϕ equal to 1. From the results given in Table 6 and Table 7, it is then possible to calculate the initial internal surface area per unit volume S_0 of PEL850. Its value is obtained by dividing the value of K_0 from Table 7 by the value of $[M_c A_{GM} / (\rho_c X_c)]$ from Table 6. Thus, S_0 was found to be $6.55 \cdot 10^6 \text{ m}^2 \cdot \text{m}^{-3}$ which is close to the value of the external surface area S_{p0} considering an initial radius r_g .

3.4.3. Comparison between the two models

Comparing the kinetic parameters obtained with the GM and the RPM, it can be seen that activation energies and reaction orders with respect to oxygen are similar for both models. This indicates that the difference arises from the values of pre-exponential factor and φ parameters.

Another aspect is that the value of $\min_x \|f(x)\|_2^2$ is slightly smaller for the RPM than the GM. This indicates a more accurate modelling for the RPM compared to the GM. However, the larger amount of unknown kinetic parameters to identify for the RPM can explain the superior precision during the modelling. To our viewpoint, the difference between the two models is negligible and the RPM does not lead to a better accuracy of the modelling. Finally, considering its less number of unknown kinetic parameters, the GM can be chosen to represent the combustion kinetic of PEL850.

Moreover, since the differential equations system including the response time of the TGA and the GM well represents the TGA data and the maximum combustion rate (Fig. 9), it can be concluded that this maximum is only due to the switching gas method during the isothermal combustion in TGA.

3.4.4. Effect of oxygen diffusion within the crucible

This section aims to verify whether the diffusion of oxygen in the crucible plays a significant role during isothermal char combustion in TGA.

By considering a uniform concentration of oxygen in the char layer, the oxygen balance in the char layer leads to the following equation:

$$\left(\begin{array}{c} \text{Accumulation of oxygen} \\ \text{in the char layer} \end{array} \right) = \left(\begin{array}{c} \text{Flux of oxygen} \\ \text{consumed by the reaction} \end{array} \right) + \left(\begin{array}{c} \text{Flux of oxygen} \\ \text{entering the charlayer} \end{array} \right) \quad (19)$$

$$\varepsilon \delta_c \cdot S_{crucible} \cdot \frac{dC_{O_2}^s}{dt} = -n_0 \cdot \frac{dX}{dt} + S_{crucible} \cdot K_c \cdot (C_{O_2}^\infty - C_{O_2}^s)$$

where ε is the porosity of the char layer ($\varepsilon = 0.4$), $S_{crucible}$ is the crucible surface (m^2), $C_{O_2}^s$ and $C_{O_2}^\infty$ are the oxygen concentration at the surface of the char particles and in the bulk respectively (mol/m^3), n_0 is the initial amount of char (mol) and K_c is the global oxygen transfer coefficient (m/s).

In Section 2.3.3., it has been demonstrated that, during char combustion in TGA, oxygen transfer effects through convection at

the upper surface of the crucible can be neglected compared to oxygen diffusion within the stagnant zone in the crucible. Consequently, the oxygen transfer coefficient can be expressed as follow:

$$K_c = \frac{D_{O_2-N_2}}{H - \delta_c} \quad (20)$$

where $D_{O_2-N_2}$ is the diffusion coefficient of oxygen into nitrogen (m^2/s). This diffusion coefficient is dependent on the combustion temperature and is calculated from ref [57].

Fig. 12(A) presents the conversion rate versus time for the intrinsic GM and the GM taking into account oxygen diffusion given in Eq. (19) during the isothermal combustion of char at 350 °C. At 350 °C, oxygen diffusion in the stagnant zone within the crucible yields to a decrease of the char reactivity. This effect is increased by raising the combustion temperature. A parameter θ is defined by the following equation:

$$\theta = \frac{t_{50\%}(GM + OD) - t_{50\%}(GM)}{t_{50\%}(GM)} \quad (21)$$

where $t_{50\%}$ is the time at 50% of conversion for the intrinsic GM and the GM plus oxygen diffusion (GM + OD). This parameter highlights the effect of oxygen diffusion within the stagnant zone during char combustion. A low value of parameter θ indicates a small impact of mass transfer on the char combustion.

Several authors in the literature [52] have considered diffusion of oxygen in the interstitial space within the char layer. This effect is considered by adding a second resistance to oxygen diffusion in the stagnant zone to represent oxygen balance. In this case, the global mass transfer coefficient is expressed using the following equation:

$$K_c = \left(\frac{H - \delta_c}{D_{O_2-N_2}} + \frac{\delta_c}{\varepsilon/\tau \cdot D_{O_2-CO_2}} \right)^{-1} \quad (22)$$

where τ is the tortuosity and $D_{O_2-CO_2}$ is the diffusion coefficient of oxygen into carbon dioxide (m^2/s). For fixed bed particles, a value of $\tau = \sqrt{2}$ can be assumed [58]. Fig. 12(A) also presents the conver-

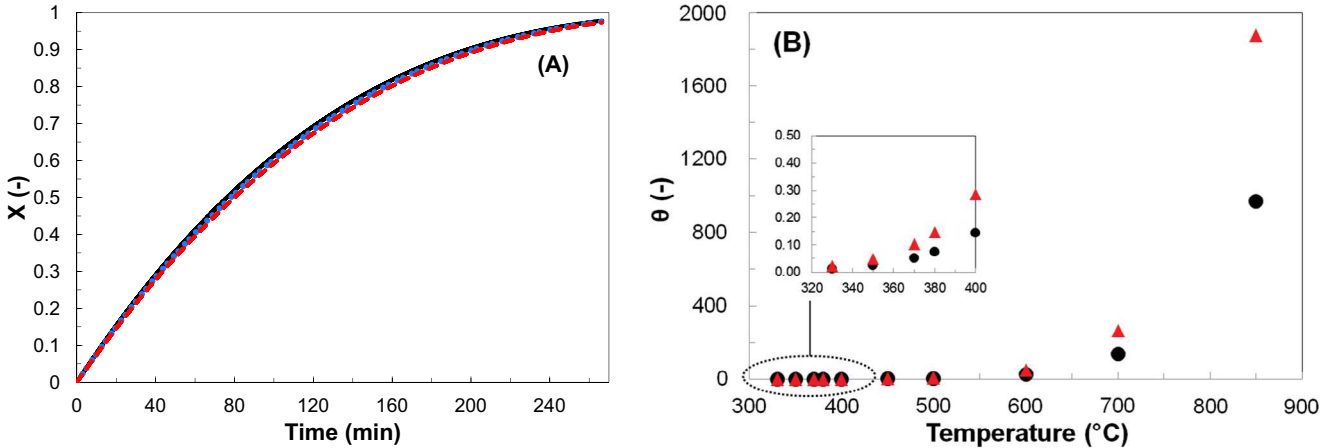


Fig. 12. Isothermal combustion of char: (A) Comparison between intrinsic GM (—), GM with oxygen diffusion in the stagnant zone (••) and (—•) GM with oxygen diffusion in the stagnant zone and within the char layer, combustion at 350 °C, (B) effect of oxygen transfer versus temperature, (●) Oxygen transfer through diffusion in the stagnant zone, (▲) oxygen transfer through diffusion in the stagnant zone and within the char layer.

sion rate versus time for the GM plus oxygen diffusion considering the global mass transfer coefficient given in Eq. (22).

Fig. 12(B) shows the effect of combustion temperature on parameter θ . It can be seen that for temperatures up to 400 °C, this parameter is less than 0.2. In this range of temperatures, effect of oxygen transfer considering either the diffusion in the stagnant or the diffusion in the stagnant zone and within the char layer can be neglected compared to intrinsic chemical reaction. The chemical reaction is very slow and is the limiting step. This figure confirms that Regime I occurs for temperatures less than 400 °C. For temperatures above 400 °C, parameter θ progressively increases before soaring above 700 °C. For these temperatures, oxygen diffusion within the crucible and in the char layer can no longer be neglected and strongly decreases char reactivity. Hence, both the intrinsic chemical reaction and mass transfer diffusion must be taken into consideration.

It is important to note that heat balance in the crucible was not considered in Fig. 12 since only the influence of oxygen transfer is studied. For temperatures under 400 °C, it was demonstrated in Section 3.1. that char combustion takes place in isothermal conditions. However, above 400 °C, heat balance should also be considered to carefully represent the char combustion.

4. Conclusion

This paper presented a kinetic study on the isothermal combustion of biomass char in TGA. The char was obtained from fast pyrolysis of beech bark pellet in a fluidized bed reactor at 850 °C. Isothermal conditions were achieved by switching the gas from inert to reactive at the desired combustion temperature in the TGA.

First, mass transfer effects in the TGA were thoroughly characterized. By analyzing the oxygen concentration at the outlet of the TGA just after the switching gas method, the oxygen partial pressure was found to be non-uniform for 25 min. Consequently, a transfer function was determined and taken into consideration in the kinetic modelling. Besides, our results showed that the mass transfer limitations mainly occur through diffusion inside the stagnant zone in the crucible.

Isothermal combustions were performed in TGA with grinded char particles. Kinetic study was carried out in Regime I in the absence of any mass transfer limitations. This Regime takes place for temperatures up to 400 °C, oxygen partial pressure ranging from 5065 to 21,273 Pa and a char particles size of 25 μm .

A comparison between the Grain Model and the Random Pore Model including the transfer function of the TGA showed that the maximum combustion rate commonly observed during char combustion in the literature is only due to the non-uniform oxygen partial pressure at the initial stage of the reaction. By considering the response time of the TGA in the kinetic modelling, kinetic parameters were determined and the Grain Model was found to well represent experimental kinetic data. Value of activation energy was equal to 124 kJ/mol. Reaction order with respect to oxygen was found to be 0.74.

Acknowledgment

The authors thank the “Midi-Pyrénées Region” for financial support of this project.

References

- [1] Di Blasi C. Modeling chemical and physical processes of wood and biomass pyrolysis. *Prog Energy Combust Sci* 2008;34:47–90.
- [2] Bridgwater AV. The technical and economic feasibility of biomass gasification for power generation. *Fuel* 1995;74:631–53.
- [3] Warnecke R. Gasification of biomass: comparison of fixed bed and fluidized bed gasifier. *Biomass Bioenergy* 2000;18:489–97.
- [4] Mahinpey N, Gomez A. Review of gasification fundamentals and new findings: Reactors, feedstock, and kinetic studies. *Chem Eng Sci* 2016;148:14–31.
- [5] Ruiz JA, Juárez MC, Morales MP, Muñoz P, Mendivil MA. Biomass gasification for electricity generation: Review current technology barriers. *Renew Sustain Energy Rev* 2013;18:174–83.
- [6] Hofbauer H, Rauch R, Löffler G, Kaiser S. Six years experience with the FICFB-gasification process, na.; 2002.
- [7] Laurendeau NM. Heterogeneous kinetics of coal char gasification and combustion. *Prog Energy Combust Sci* 1978;4:221–70.
- [8] Szekely J, Evans JW, Sohn HY. Gas-solid reactions. Elsevier; 2012.
- [9] Morin M, Pécate S, Hémati M, Kara Y. Pyrolysis of biomass in a batch fluidized bed reactor: effect of the pyrolysis conditions and the nature of the biomass on the physicochemical properties and reactivity of char. *J Anal Appl Pyrol* 2016;122:511–23.
- [10] Guerrero M, Ruiz MP, Alzueta MU, Bilbao R, Millera A. Pyrolysis of eucalyptus at different heating rates: studies of char characterization and oxidative reactivity. *J Anal Appl Pyrol* 2005;74:307–14.
- [11] Cetin E, Moghtaderi B, Gupta R, Wall TF. Influence of pyrolysis conditions on the structure and gasification reactivity of biomass char. *Fuel* 2004;83:2139–50.
- [12] Kumar M, Gupta RC. Influence of carbonization conditions on the gasification of acacia and eucalyptus wood chars by carbon dioxide. *Fuel* 1994;73:1922–5.
- [13] Fushimi C, Araki K, Yamaguchi Y, Tsutsumi A. Effect of heating rate on steam gasification of biomass. 1. Reactivity of char. *Ind Eng Chem Res* 2003;42:3922–8.
- [14] Mermoud F, Salvador S, Van de Steene L, Golfier F. Influence of the pyrolysis heating rate on the steam gasification rate of large wood char particles. *Fuel* 2006;85:1473–82.
- [15] Okumura Y, Hanaoka T, Sakanishi K. Effect of pyrolysis conditions on gasification reactivity of woody biomass-derived char. *Proc Combust Inst* 2009;32:2013–20.
- [16] Zanzi R, Sjöström K, Björnborn E. Rapid high-temperature pyrolysis of biomass in a free-fall reactor. *Fuel* 1996;75:545–50.
- [17] Várhegyi G, Mészáros E, Antal MJ, Bourke J, Jakab E. Combustion kinetics of corn cob charcoal and partially demineralized corn cob charcoal in the kinetic regime. *Ind Eng Chem Res* 2006;45:4962–70.
- [18] Kovacic G, Chambers A, Özüim B. CO₂ gasification kinetics of two alberta coal chars. *Can J Chem Eng* 1991;69:811–5.
- [19] Magnaterra M, Fusco JR, Ochoa J, Cukierman AL. Kinetic study of the reaction of different hardwood sawdust chars with oxygen. Chemical and structural characterization of the samples. *Adv Thermochem Biomass Convers* 1993;116–30.
- [20] Adánez J, de Diego LF, García-Labiano F, Abad A, Abanades JC. Determination of biomass char combustion reactivities for FBC applications by a combined method. *Ind Eng Chem Res* 2001;40:4317–23.
- [21] Janse AMC, de Jonge HG, Prins W, van Swaij WPM. Combustion kinetics of char obtained by flash pyrolysis of pine wood. *Ind Eng Chem Res* 1998;37:3909–18.
- [22] Di Blasi C, Buonanno F, Branca C. Reactivities of some biomass char in air. *Carbon* 1999;37:1227–38.
- [23] Cozzani V. Reactivity in oxygen and carbon dioxide of char formed in the pyrolysis of refuse-derived fuel. *Ind Eng Chem Res* 2000;39:864–72.
- [24] Kashiwagi T, Nambu H. Global kinetic constant for thermal oxidative degradation of a cellulosic paper. *Combust Flame* 1992;88:345–68.
- [25] Luo M, Stanmore B. The combustion characteristics of char from pulverized bagasse. *Fuel* 1992;71:1074–6.
- [26] Standish N, Tanjung AFA. Gasification of single wood charcoal particle in CO₂. *Fuel* 1988;67:666–72.
- [27] Ye DP, Agnew JB, Zhang DK. Gasification of a South Australian low-rank coal with carbon dioxide and steam: kinetic and reactivity studies. *Fuel* 1998;77:1209–19.
- [28] Zolin A, Jensen A, Jensen PA, Frandsen F, Dam-Johansen K. The influence of inorganic materials on the thermal deactivation of fuels chars. *Energy Fuels* 2001;15:1110–22.
- [29] Asadullah M, Zhang S, Min Z, Yimsiri P, Li CZ. Effect of biomass char structure on its gasification reactivity. *Bioresour Technol* 2010;101:7935–43.
- [30] Hurt RH, Calo JM. Semi-global intrinsic kinetics for char combustion modeling. *Combust Flame* 2001;125:1138–49.
- [31] Vyazovkin S, Burnham AK, Criado JM, Pérez-Maquada LA, Popescu C, Sbirrazzuoli N. ICTAC kinetic committee recommendations for performing kinetic computations on thermal analysis data. *Thermochim Acta* 2011;520:1–19.
- [32] Khawam A, Flanagan DR. Solid-state kinetic models: basics and mathematical fundamentals. *J Phys Chem B* 2010;110:17315–28.
- [33] Di Blasi C. Combustion and gasification rates of lignocellulosic chars. *Prog Energy Combust Sci* 2009;35:121–40.
- [34] Essenhigh RH. Rate equations for the carbon-oxygen reaction: an evaluation of the Langmuir Adsorption Isotherm at atmospheric pressure. *Energy Fuels* 1991;5:41–6.
- [35] Essenhigh RH. Influence of pressure on the combustion rate of carbon. Twenty-Sixth Symp Combust 1996:3085–94.
- [36] Murphy JJ, Shaddix CR. Combustion kinetics of coal chars in oxygen-enriched environments. *Combust Flame* 2006;144:710–29.
- [37] Dutta S, Wen CY. Reactivity of coal and char. 2. In oxygen-nitrogen atmosphere. *Ind Eng Chem Process Des Dev* 1977;16:31–7.

- [38] Wen CY. Noncatalytic heterogeneous solid fluid reaction models. *Ind Eng Chem* 1968;60:34–54.
- [39] Irfan MF, Usman MR, Kusakabe K. Coal gasification in CO₂ atmosphere and its kinetics since 1948: a brief review. *Energy* 2011;36:12–40.
- [40] Hemati M. Etude de la pyrolyse et de la gazéification de bois thermogravimétrie et en lit fluidisé de catalyseur [Ph.D. thesis]. Institut National Polytechnique de Toulouse; 1984.
- [41] Bathia SK, Perlmutter DD. A random pore model for fluid-solid reaction: I. Isothermal, kinetic control. *AIChE J* 1980;26:379–86.
- [42] Septien S, Escudero Sanz FJ, Salvador S, Valin S. Steam gasification of char from wood chips fast pyrolysis: development of a semi-empirical model for a fluidized bed reactor application. *Biomass Bioenergy* 2015;77:64–74.
- [43] Azharul Islan Md, Auta M, Kabir G, Hameed BH. A thermogravimetric analysis of the combustion kinetics of karanja (*Pongamia pinnata*) fruit hulls char. *Bioresour Technol* 2016;200:335–41.
- [44] Branca C, Di Blasi C. Global kinetics of wood char devolatilization and combustion. *Energy Fuels* 2003;17:1609–15.
- [45] Barrio M, Gøbel B, Risnes H, Henriksen U, Hustad JE, Sørensen LH. Steam gasification of wood char and the effect of hydrogen inhibition on the chemical kinetics. In: *Conference on progress in thermochemical biomass conversion*; 2001.
- [46] Gomez A, Silbermann R, Mahinpey N. A comprehensive experimental procedure for CO₂ coal gasification: is there really a maximum reaction rate? *Appl Energy* 2014;124:73–81.
- [47] Zeng X, Wang F, Wang Y, Li A, Yu J, Xu G. Characterization of char gasification in a micro fluidized bed reaction analyzer. *Energy Fuels* 2014;28:1838–45.
- [48] Klinghoffer NB, Castaldi MJ, Nzihou A. Catalyst properties and catalytic performance of char from biomass gasification. *Ind Eng Chem Res* 2012;51:13113–22.
- [49] Gomez A, Mahinpey N. Kinetic study of coal steam and CO₂ gasification: a new method to reduce interparticle diffusion. *Fuel* 2015;148:160–7.
- [50] Ollero P, Serrera A, Arjona R, Alcantarilla S. Diffusional effects in TGA gasification experiments for kinetic determination. *Fuel* 2002;81:1989–2000.
- [51] Gómez-Barea A, Ollero P, Arjona R. Reaction-diffusion model of TGA gasification experiments for estimating diffusional effects. *Fuel* 2005;84:1695–704.
- [52] Schulze S, Nikrityuk P, Abosteif Z, Guhl S, Richter A, Meyer B. Heat and mass transfer within thermogravimetric analyser: from simulation to improved estimation of kinetic data for char gasification. *Fuel* 2017;187:338–48.
- [53] Boynton WP, Brattain WH. Interdiffusion of gases and vapors. *Int Crit Tables* 1929;5:62–3.
- [54] Khawam A, Flanagan DR. Role of isoconversional methods in varying activation energies of solid-state kinetics I. isothermal kinetic studies. *Thermochim Acta* 2005;429:93–102.
- [55] Feroso J, Gil MV, García S, Pevida C, Pis JJ, Rubiera F. Kinetic parameters and reactivity for the steam gasification of coal chars obtained under different pyrolysis temperatures and pressures. *Energy Fuels* 2011;25:3574–80.
- [56] Kajitani S, Hara S, Matsuda H. Gasification rate analysis of coal char with a pressurized drop tube furnace. *Fuel* 2002;81:539–46.
- [57] Bird RB, Stewart WE, Lightfoot EN. *Transport phenomena*. 2nd ed. Wiley; 2002.
- [58] Dullien FAL. *Porous media: fluid transport and pore structure*. 2nd ed. Academic Press; 2012.